Volume 53
Number 45
7 December 2024
Pages 18057-18386

Dalton Transactions

An international journal of inorganic chemistry

rsc.li/dalton

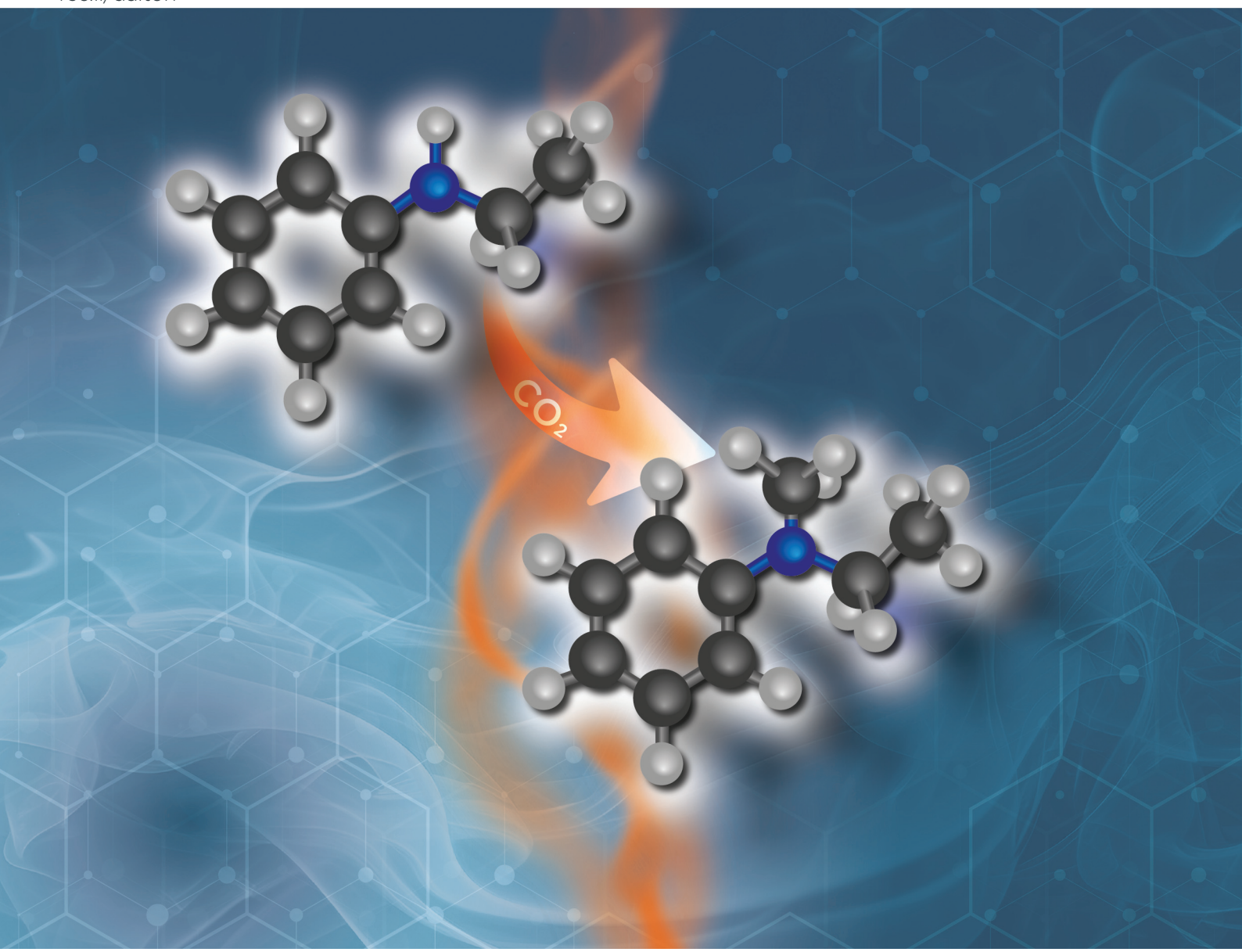

ISSN 1477-9226

ROYAL SOCIETY OF CHEMISTRY

PAPER

Cristina Tubaro, Marco Baron *et al.*

Exploring the reductive CO_2 fixation with amines and hydrosilanes using readily available Cu(II) NHC–phenolate catalyst precursors

Dalton Transactions

ROYAL SOCIETY OF CHEMISTRY

PAPER

View Article Online
View Journal | View Issue

Cite this: *Dalton Trans.*, 2024, **53**, 18128

Exploring the reductive CO_2 fixation with amines and hydrosilanes using readily available Cu(II) NHC–phenolate catalyst precursors†

Giammarco Meloni,[a,b] Luca Morgan,[a] David Cappelletti,[a] Matteo Bevilacqua,[a] Claudia Graiff,[c] Piermaria Pinter,[d] Andrea Biffis,[a,b] Cristina Tubaro *[a,b] and Marco Baron *[a,b]

Received 21st October 2024,
Accepted 23rd October 2024

DOI: 10.1039/d4dt02936d

rsc.li/dalton

N-Methylation of amines is of great interest in the synthesis of pharmaceuticals and valuable compounds, and the possibility to perform this reaction with an inexpensive and non-toxic substrate like CO_2 and its derivatives is quite appealing. Herein, the synthesis of four novel homoleptic Cu(II) complexes with hybrid NHC–phenolate (NHC = *N*-Heterocyclic Carbene) ligands is reported, and their use in the catalytic *N*-methylation of amines with CO_2 in the presence of hydrosilanes is explored. Both bidentate or tetradentate ligands can be used in the preparation of the complexes provided that the structural requirement that the two NHC and the two phenolate donors in the metal coordination sphere are mutually in *trans* is fulfilled. A new reaction protocol to perform the *N*-methylation of secondary aromatic amines and dibenzylamine in high yield under mild reaction conditions is developed, using the ionic liquid [BMMIM][NTf_2] (1-butyl-2,3-dimethylimidazolium bis(trifluoromethylsulfonyl)imide) as solvent and the catalyst precursor **[Cu(L^2)$_2$]**. Reactivity studies indicate that the reaction follows two different pathways with different hydrosilanes, and that the starting Cu(II) complexes are reduced under the catalytic conditions.

Introduction

Copper has always attracted considerable interest in coordination chemistry, especially in its monovalent (+1) and bivalent (+2) oxidation states. A plethora of different applications with copper-containing compounds, ranging from catalysis, to medicinal and agricultural chemistry is documented in the literature.[1–5] Even though most of the reported studies involve nitrogen- and phosphorus-based ligands, copper complexes with *N*-Heterocyclic Carbene ligands (NHCs) are increasingly getting more studied, following the first report by Arduengo in 1993.[6] The NHCs, thanks to their soft character, prefer to coordinate to the softer Cu(I) rather than to the borderline–hard Cu(II) metal centre. Fundamental contributions in the field of homogeneous catalysis with Cu(I) NHC complexes were reported by the groups of Hoveyda,[7–11] Nolan,[12–15] and Cazin.[16–18] A huge variety of organic reactions is catalysed by Cu(I) NHC complexes,[19] and exceptional results in terms of stability, activity, regio- and enantioselectivity are achieved, if compared to the similar phosphine-based Cu(I) complexes.[18,20,21] Thanks to the copper natural abundance and low toxicity,[22–24] Cu(I) NHCs are more environmentally sustainable catalysts compared to those commonly adopted in organometallic chemistry (*e.g.* platinum group metals). Furthermore, thanks to the d^{10} ground state configuration, Cu(I) NHC complexes exhibit high-quality photophysical properties: the fast nonradiative decay towards low-lying metal-centred states is absent and they can be applied for their fluorescence or phosphorescence properties.[25–31] Instead, the chemistry of Cu(II) NHCs has been less explored and a lower number of complexes has been reported to date.[32–42] The first Cu(II) NHC complex was reported by Meyer's group in 2003, with an hybrid tripodal NHC-imine ligand (NHC–N).[32] Thanks to the hybrid nature of the ligand the resulting complex is air stable in the solid state, a marked difference compared to monodentate NHC Cu(II) complexes, which in general are moisture and water sensitive.[35] A similar behaviour is observed with several hybrid multidentate NHC–N and NHC–O ligands. Among them, although the examples of Cu(II) complexes with NHC–phenolates (NHC–O) are limited

[a]*Dipartimento di Scienze Chimiche, Università degli Studi di Padova, via Marzolo 1, 35131 Padova, Italy. E-mail: cristina.tubaro@unipd.it, marco.baron@unipd.it*
[b]*Consorzio Interuniversitario per le Reattività Chimiche e la Catalisi, Unità di Ricerca di Padova, via Marzolo 1, 35131 Padova, Italy*
[c]*Dipartimento di Scienze Chimiche, della Vita e della Sostenibilità Ambientale, Università degli Studi di Parma, Parco Area delle Scienze 17/A, 43124 Parma, Italy*
[d]*Novaled GmbH, Elisabeth-Boer-Straße 9, 01099 Dresden, Germany*

†Electronic supplementary information (ESI) available: NMR, FT-IR, UV-Vis and ESI-MS spectra, SC-XRD and computational details, additional catalytic data, stoichiometric reactions NMR spectra. CCDC 2371863 and 2371864. For ESI and crystallographic data in CIF or other electronic format see DOI: https://doi.org/10.1039/d4dt02936d

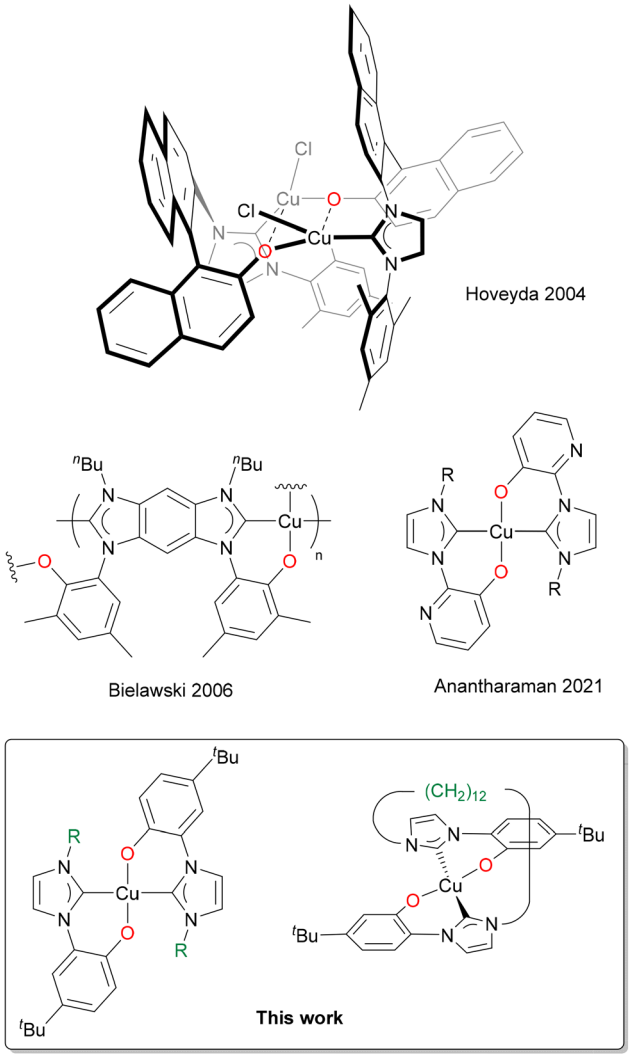

Scheme 1 Cu(II) NHC–phenolate complexes reported in the literature (top), and in this study (bottom).[43–45]

(Scheme 1),[43–45] they have been recently reported to be air and moisture stable.[43]

One interesting catalytic reaction is the reductive *N*-formylation and *N*-methylation of amines with CO_2 or formic acid in the presence of hydrosilanes. In this frame it is worth mentioning that in industrial processes the Eschweiler–Clarke reaction, using formaldehyde as the C1 source, prevails among the *N*-methylation of amine methodologies,[46–49] and it is still an active research area,[50–53] considering that *N*-methylation of amines is of great interest in the synthesis of pharmaceuticals and valuable compounds.[54,55] Anyway, the possibility to perform this reaction with an inexpensive and non-toxic substrate like CO_2 and its derivatives is quite appealing.[56–63]

The reductive *N*-formylation and *N*-methylation of amines with CO_2 or formic acid in the presence of hydrosilanes was first reported by Cantat in 2013 catalysed by Zn(II) salts in combination with neutral donor ligands, such phosphines and NHCs.[56] Organocatalysts, such as free NHCs, are also active in this transformation.[64]

Cu(I) NHC complexes were also reported to be active in this reaction but, to the best of our knowledge, Cu(II) NHC complexes have never been studied yet. Up to now, in fact only Cu(II) metal salts in combination with phosphine ligands have been reported as catalysts for the cited reaction.[65–68] In this work we report the synthesis of three novel bidentate NHC–phenolate and one tetradentate bis(NHC)–bis(phenolate) ligand precursors, and their corresponding Cu(II) complexes (Scheme 1). The catalytic activity of the complexes in the reductive *N*-formylation/*N*-methylation of amines with CO_2 and hydrosilanes is also explored, by comparing the activity with mono- and bis(NHC) Cu(I) complexes and through a reactivity study aimed at shedding light on the possible active species involved in the catalytic process. We can anticipate that the catalytic performance of the Cu(II) complexes is superior in terms of *N*-methylated product yield compared to what we observed in previous studies with Mn(I) complexes, even working under milder conditions.[59]

Experimental

Materials and methods

Unless specified otherwise, all manipulations were performed under argon atmosphere using standard Schlenk techniques, and all the utilized glassware was oven-dried at 110 °C prior to use. Methanol, dichloromethane, and *n*-hexane used for synthesis were argon-degassed and stored under inert gas and molecular sieves. All the solvents used for catalytic tests were stored over molecular sieves and degassed by three consecutive freeze–pump–thaw cycles before their use. All the chemicals were purchased from commercial supplier and used without further purification. 1-(5-*tert*-butyl-2-methoxyphenyl)-imidazole was prepared following reported literature procedures.[69,70] NMR spectra were recorded at 298 K on a Bruker Avance 300 MHz, operating at 300.1, 75.5 and 121.5 MHz, respectively for ^{1}H, ^{13}C and ^{31}P NMR nuclei. Chemical shifts are reported in parts per million and calibrated respect to the solvent residue. ^{1}H NMR signals are labelled as s = singlet, d = doublet, t = triplet, q = quartet, quint = quintet, sept = septet, m = multiplet and br = broad. ESI mass spectra were recorded on a Finnigan Thermo LCQ-Duo ESI mass spectrometer operating in positive ion mode; sample solutions were prepared by dissolving the compounds in acetonitrile and were directly infused into the ESI source by a syringe pump at 8 μL min^{-1} flow rate. Elemental analyses were performed by the microanalytical laboratory of Chemical Sciences Department (University of Padova) with a ThermoScientific FLASH 2000 elemental analyzer. FT-IR spectra were recorded at 25 °C, with a Bruker Tensor 27 spectrometer, preparing KBr pellets for the samples. The IR spectra were recorded in the mid-infrared using a 4000–400 cm^{-1} wavenumber range and a spectral resolution of 2 cm^{-1}. Absorption peaks are labelled based on their intensity,

vs = very strong, s = strong, m = medium, w = weak, vw = very weak, b = broad. UV-vis absorption spectra were recorded in dichloromethane at 25 °C using a Varian Cary 100 Bio spectrophotometer, with 1 cm optical path quartz cells, from 900 to 190 nm after baseline correction.

Synthesis of the proligands

General procedure for the synthesis of $Ha^{1-2}Br$ and $Ha^{3}I$. In a Schlenk tube, a solution of 1-(5-*tert*-butyl-2-methoxyphenyl)-imidazole (2.2 mmol, 1 equiv.) and the respective alkyl halide (4 equiv.) in 10 mL acetonitrile, was heated at 80 °C for 16 h. The solvent was then removed, and the residue was treated with diethyl ether (15 mL), collected by filtration, washed with diethyl ether (3 × 15 mL) and dried under reduced pressure.

$Ha^{1}Br$ – alkyl halide: benzyl bromide, Yield: 95% (white solid). ^{1}H NMR (300.1 MHz, DMSO-d_6): δ = 9.80 (s, 1H, NCHN), 8.08 (s, 1H, NCH), 8.00 (s, 1H, NCH), 7.64–7.27 (m, 8H, Ar), 5.54 (s, 2H, CH_2), 3.85 (s, 3H, OCH_3), 1.30 (s, 9H, CH_3) ppm. ^{13}C NMR (75.5 MHz, DMSO-d_6): δ = 149.9 (Ar), 143.9 (Ar), 137.3 (NCHN), 134.6 (Ar), 129.0 (Ar), 128.9 (Ar), 128.5 (Ar), 128.3 (Ar), 124.3 (NCH), 123.2 (Ar), 122.8 (Ar), 122.0 (NCH), 112.8 (Ar), 56.4 (CH_2), 52.2 (OCH_3), 34.2 (C), 31.1 (CH_3) ppm.

$Ha^{2}Br$ – alkyl halide: 1-bromohexane, Yield: 91% (hygroscopic white solid). ^{1}H NMR (300.1 MHz, DMSO-d_6): δ = 9.56 (s, 1H, NCHN), 8.07 (t, J = 1.7 Hz, 1H, NCH), 8.00 (t, J = 1.7 Hz, 1H, NCH), 7.63–7.57 (m, 2H, Ar), 7.28 (d, J = 9.5 Hz, 1H, Ar), 4.25 (t, J = 7.2 Hz, 2H, NCH_2), 3.84 (s, 3H, OCH_3), 1.87 (quint, J = 7.2 Hz, 2H, CH_2), 1.30 (m, 15H, CH_3 + CH_2), 0.87 (t, J = 6.5 Hz, 3H, hex-CH_3) ppm. ^{13}C NMR (75.5 MHz, DMSO-d_6): δ = 150.0 (Ar), 143.9 (Ar), 137.1 (NCHN), 128.3 (Ar), 124.0 (NCH), 123.3 (Ar), 122.9 (Ar), 122.1 (NCH), 112.9 (Ar), 56.4 (OCH_3), 49.2 (NCH_2), 34.2 (C), 31.1 (CH_3), 30.6 (CH_2), 29.2 (CH_2), 25.2 (CH_2), 22.0 (CH_2), 13.9 (hex-CH_3) ppm.

$Ha^{3}I$ – alkyl halide: methyl iodide, Yield: 93% (hygroscopic light–yellow solid). ^{1}H NMR (300.1 MHz, DMSO-d_6): δ = 9.49 (s, 1H, NCHN), 8.04 (s, 1H, NCH), 7.90 (s, 1H, NCH), 7.61–7.58 (m, 2H, Ar), 7.28 (d, J = 9.5 Hz, 1H, Ar), 3.95 (s, 3H, NCH_3), 3.85 (s, 3H, OCH_3), 1.30 (s, 9H, CH_3) ppm. ^{13}C NMR (75.5 MHz, DMSO-d_6): δ = 149.9 (Ar), 143.9 (Ar), 137.6 (NCHN), 128.2 (Ar), 123.7 (NCH), 123.3 (NCH), 123.2 (Ar), 122.8 (Ar), 112.8 (Ar). 56.4 (OCH_3), 36.0 (NCH_3), 34.1 (C), 31.0 (CH_3) ppm.

Synthesis of $H_2a^{4}Br_2$. In a pressure tube, a mixture of 1-(5-*tert*-butyl-2-methoxyphenyl)-imidazole (2.2 mmol, 1 equiv.) and 1,12-dibromododecane (1.0 mmol, 0.5 equiv.) was stirred and heated at 120 °C for 16 h. The crude product was treated with diethyl ether (10 mL) at room temperature, obtaining a white solid that was successively collected by filtration, washed three times with diethyl ether and dried under vacuum.

$H_2a^{4}Br_2$ – Yield: 94% (brownish solid). ^{1}H NMR (300.1 MHz, DMSO-d_6): δ = 9.62 (t, J = 1.5 Hz, 2H, NCHN), 8.07 (t, J = 1.5 Hz, 2H, NCH), 8.00 (t, J = 1.5 Hz, 2H, NCH), 7.60–7.58 (m, 4H, Ar), 7.28 (d, J = 9.5 Hz, 2H, Ar), 4.27 (t, J = 7.4 Hz, 4H, NCH_2), 3.84 (s, 6H, OCH_3), 1.87 (br, 4H, CH_2), 1.30–1.26 (m, 34H, CH_3 + CH_2) ppm. ^{13}C NMR (75.5 MHz, DMSO-d_6): δ = 150.0 (Ar), 144.0 (Ar), 137.1 (NCHN), 128.3 (Ar), 123.9 (NCH), 123.2 (Ar), 122.9 (Ar), 122.2 (NCH), 112.9 (Ar), 56.4 (OCH_3), 49.2 (NCH_2), 34.2 (C), 31.1 (CH_3), 29.3 (CH_2), 29.0 (CH_2), 28.9 (CH_2), 28.4 (CH_2), 25.6 (CH_2) ppm.

General procedure for the synthesis of $H_2L^{1-2}Br$, $H_2L^{3}I$, and $H_4L^{4}Br_2$. The precursors **$Ha^{1-2}Br$**, **$Ha^{3}I$**, or **$H_2a^{4}Br_2$** (2.0 mmol) was dissolved in 15 mL of a 1 : 1 HBr : acetic acid mixture and heated at 125 °C for 16 h. The solvent was then removed at reduced pressure, and the product recrystallized from acetone/diethyl ether, washed with diethyl ether (3 × 15 mL) and dried under reduced pressure.

$H_2L^{1}Br$ – Yield: 80% (light brown solid). ^{1}H NMR (300.1 MHz, DMSO-d_6): δ = 10.62 (s, 1H, OH), 9.86 (s, 1H, NCHN), 8.09 (s, 1H, NCH), 8.03 (s, 1H, NCH), 7.56–7.10 (m, 7H, Ar), 7.11 (d, J = 8.5 Hz, 1H, Ar), 5.58 (s, 2H, NCH_2), 1.28 (s, 9H, CH_3) ppm. ^{13}C NMR (75.5 MHz, DMSO-d_6): δ = 148.1 (Ar), 142.5 (Ar), 137.0 (NCHN), 134.8 (Ar), 129.0 (Ar), 128.8 (Ar), 128.5 (Ar), 128.0 (Ar), 124.0 (NCH), 122.5 (Ar), 122.0 (Ar), 121.6 (NCH), 116.7 (Ar), 52.0 (NCH_2), 34.0 (C), 31.1 (CH_3) ppm. FT-IR $\bar{\nu}$: 3062 (vs), 2960 (s), 1622 (m), 1549 (s), 1513 (s), 1456 (m), 1363 (m), 1274 (s), 1139 (m), 1072 (m), 823 (s), 710 (vs), 650 (m), 472 (w) cm^{-1}.

$H_2L^{2}Br$ – Yield: 85% (hygroscopic white solid). ^{1}H NMR (300.1 MHz, DMSO-d_6): δ = 10.60 (s, 1H, OH), 9.67 (s, 1H, NCHN), 8.07 (s, 1H, NCH), 8.00 (s, 1H, NCH), 7.50–7.41 (m, 2H, Ar), 7.12 (d, J = 8.50 Hz, 1H, Ar), 4.30 (t, J = 7.2 Hz, 2H, NCH_2), 1.87 (br, 2H, CH_2), 1.27 (br, 15H, CH_3 + CH_2), 0.85 (s, 3H, hex-CH_3) ppm. ^{13}C NMR (75.5 MHz, DMSO-d_6): δ = 148.2 (Ar), 142.5 (Ar), 136.8 (NCHN), 128.0 (Ar), 123.6 (NCH), 122.6 (Ar), 122.1 (NCH), 121.7 (Ar), 116.7 (Ar), 49.1 (NCH_2), 34.0 (C), 31.1 (CH_3), 30.6 (CH_2), 29.3 (CH_2), 25.2 (CH_2), 21.9 (CH_2), 13.9 (hex-CH_3) ppm.

$H_2L^{3}Br$ – Yield: 92% (hygroscopic light yellow solid). ^{1}H NMR (300.1 MHz, DMSO-d_6): δ = 10.60 (s, 1H, OH), 9.48 (s, 1H, NCHN), 8.04 (t, J = 1.8 Hz, 1H, NCH), 7.88 (t, J = 1.8 Hz, 1H, NCH), 7.47–7.42 (m, 2H, Ar), 7.07 (d, J = 8.5 Hz, 1H, Ar), 3.95 (s, 3H, NCH_3), 1.28 (s, 9H, CH_3) ppm. ^{13}C NMR (75.5 MHz, DMSO-d_6): δ = 148.2 (Ar), 142.5 (Ar), 137.4 (NCHN), 128.1 (Ar), 123.5 (NCH), 123.3 (NCH), 122.6 (Ar), 121.7 (Ar), 116.7 (Ar), 36.0 (NCH_3), 34.0 (C), 31.1 (CH_3) ppm.

$H_4L^{4}Br_2$ – Yield: 83% (brownish solid). ^{1}H NMR (300.1 MHz, DMSO-d_6): δ = 10.59 (s, 2H, OH), 9.61 (s, 2H, NCHN), 8.07 (s, 2H, NCH), 8.01 (s, 1H, NCH), 7.49–7.42 (m, 4H, Ar), 7.09 (d, J = 8.50 Hz, 2H, Ar), 4.27 (t, J = 7.4 Hz, 4H, NCH_2), 1.87 (br, 4H, CH_2), 1.30 (br, 34H, CH_3 + CH_2) ppm. ^{13}C NMR (75.5 MHz, DMSO-d_6): δ = 148.2 (Ar), 142.5 (Ar), 136.8 (NCHN), 128.1 (Ar), 123.7 (NCH), 122.6 (NCH), 122.1 (Ar), 121.7 (Ar), 116.7 (Ar), 49.1 (NCH_2), 34.0 (C), 31.1 (CH_3), 29.3 (CH_2), 30.0 (CH_2), 28.9 (CH_2), 28.4 (CH_2), 25.6 (CH_2) ppm.

Anion metathesis on ligand precursors. The ligand precursor (0.4 mmol) was dissolved in 50 mL of water and, under stirring, a water solution of KPF_6 (4 mmol, 10 equiv., in 10 mL) was added dropwise. The mixture was stirred overnight, and the white product collected by filtration, washed with water (3 × 10 mL) and dried under reduced pressure.

$Ha^{1}PF_6$ – Starting from **$Ha^{1}Br$**, Yield: 90% (white solid). ^{1}H NMR (300.1 MHz, CD_3CN): δ = 8.92 (s, 1H, NCHN), 7.62 (s, 1H, NCH), 7.60 (m, 1H, Ar), 7.52 (s, 1H, NCH), 7.49–7.47 (m, 6H,

Ar), 5.43 (s, 2H, CH_2), 3.87 (s, 3H, OCH_3), 1.33 (s, 9H, CH_3) ppm. ^{31}P NMR (121 MHz, CD_3CN): δ = −144.62 (sept, J = 710 Hz, PF_6) ppm. ^{19}F NMR (189 MHz, CD_3CN): δ = −70.57 (d, J = 710 Hz, PF_6) ppm.

$H_2L^1PF_6$ – Starting from **H_2L^1Br**, Yield: 85% (white solid). ^{1}H NMR (300.1 MHz, CD_3CN): δ = 9.06 (s, 1H, NCHN), 7.55–7.46 (m, 10H, Ar + NCH), 7.35 (d, J = 8.4 Hz, 1H, Ar), 5.47 (s, 2H, NCH_2), 1.34 (s, 9H, CH_3) ppm. ^{31}P NMR (121 MHz, CD_3CN): δ = −144.6 (sept, J = 710 Hz, PF_6) ppm. ^{19}F NMR (189 MHz, CD_3CN): δ = −70.6 (d, J = 710 Hz, PF_6) ppm.

Synthesis of the copper complexes

General procedure for the synthesis of the Cu(II) complexes [Cu(L^1)$_2$], [Cu(L^2)$_2$], [Cu(L^3)$_2$], and [Cu(L^4)]. A mixture of $Cu(OAc)_2{\cdot}H_2O$ (0.26 mmol, 1 equiv.), K_2CO_3 (1.04 mmol, 4 equiv.), and the ligand precursor (0.52 mmol, 2 equiv.) was suspended in dry and degassed methanol (10 mL) under argon atmosphere. After 5 hours of stirring, the solvent was removed, and the purple-brown residue extracted with 10 mL of anhydrous dichloromethane. The obtained suspension was filtered *via* cannula filtration, then the volume of the remaining solution was reduced to approximatively 2 mL. Finally, after the addition of degassed *n*-hexane (15 mL), the product was recovered as a solid (powder) by filtration.

[Cu(L^1)$_2$] – Yield: 80% (dark brownish-purple powder). Elemental analysis calcd (%) for $C_{40}H_{42}CuN_4O_2{\cdot}H_2O$: C 69.39, H 6.41, N 8.09. Found: C 69.77, H 6.75, N 7.92. ESI(+)-MS (*m*/*z*): 674.17 [**[Cu(L^1)$_2$]** + H]$^+$. FT-IR $\tilde{\nu}$: 3089 (vw), 3062 (vw), 3025 (vw), 2960 (s), 2863 (w), 1610 (m), 1499 (vs), 1455 (m), 1411 (m), 1492 (w), 1356 (m), 1306 (vs), 1262 (s), 1147 (m), 1109 (w), 866 (w), 834 (s), 776 (w), 737 (s), 721 (m), 709 (m), 667 (w), 619 (vw), 595 (vw), 557 (vw), 447 (vw), 411 (vw) cm^{-1}. UV-vis (CH_2Cl_2): λ (ε/M^{-1} cm^{-1}) = 230 (44 100), 318 (14 400), 455 (970) nm. Crystals suitable for single crystal X-ray diffraction (SC-XRD) analysis were obtained by slow evaporation of a concentrated solution of the complex in acetone.

[Cu(L^2)$_2$] – Yield: 60% (purple powder). Elemental analysis calcd (%) for $C_{38}H_{54}CuN_4O_2{\cdot}1.5H_2O$: C 66.20, H 8.33, N 8.13. Found: C 66.19, H 8.42, N 8.05. ESI(+)-MS (*m*/*z*): 662.21 [**[Cu(L^2)$_2$]** + H]$^+$. FT–IR $\tilde{\nu}$: 3159 (vw), 3124 (vw), 3087 (vw), 2958 (vs), 2928 (vs), 2959 (s), 1609 (m), 1500 (vs), 1464 (m), 1392 (m), 1362 (m), 1349 (m), 1303 (vs), 1262 (s), 1148 (m), 1105 (w), 1171 (vw), 871 (w), 828 (s), 737 (s), 671 (w), 620 (vw), 595 (vw), 445 (vw), 410 (vw) cm^{-1}. UV-vis (CH_2Cl_2): λ (ε/M^{-1} cm^{-1}) = 230 (37 100), 319 (12 500), 460 (830) nm.

[Cu(L^3)$_2$] – Yield: 55% (dark brown powder). ESI(+)-MS (*m*/*z*): 522.12 [**[Cu(L^3)$_2$]** + H]$^+$. FT–IR $\tilde{\nu}$: 3174 (vw), 3145 (vw), 3063 (vw), 2958 (s), 2903 (m), 2864 (m), 1675 (w), 1609 (m), 1501 (vs), 1460 (s), 1402 (m), 1353 (m), 1315 (vs), 1264 (s), 1149 (m), 1118 (w), 1083 (w), 1020 (vw), 873 (w), 835 (s), 819 (s), 751 (s), 723 (s), 666 (m), 617 (vw), 592 (vw), 524 (vw), 445 (vw), 403 (w) cm^{-1}. UV-vis (CH_2Cl_2): λ (ε/M^{-1} cm^{-1}) = 230 (35 700), 320 (9400), 454 (580) nm.

[Cu(L^4)] – In this synthesis 0.26 mmol of **$H_4L^4Br_2$** were used (1 : 1 molar ratio between Cu and ligand precursor). Yield: 58% (dark purple powder). Elemental analysis calcd (%) for $C_{38}H_{52}CuN_4O_2{\cdot}H_2O$: C 67.28, H 8.02, N 8.26. Found: C 67.23, H 7.73, N 8.06. ESI(+)-MS (*m*/*z*): 660.26 [[Cu(L^4)] + H]$^+$. FT–IR $\tilde{\nu}$: 3171 (vw), 3135 (vw), 3069 (vw), 2952 (vs), 2925 (vs), 2854 (s), 1688 (w), 1609 (m), 1500 (vs), 1462 (m), 1414 (m), 1392 (m), 1362 (m), 1350 (m), 1315 (s), 1262 (s), 1202 (w), 1147 (m), 1107 (w), 1070 (w), 1027 (vw), 874 (w), 862 (w), 834 (s), 832 (s), 737 (m), 720 (m), 669 (m), 619 (vw), 528 (vw), 404 (w) cm^{-1}. UV-vis (CH_2Cl_2): λ (ε/M^{-1} cm^{-1}) = 230 (32 500), 318 (10 400), 465 (980) nm.

Synthesis of the copper(I) complex [CuBr(a^1)]. A mixture of **Ha^1Br** (0.25 mmol, 1 equiv.), $CuBr(SMe_2)$ (0.25 mmol, 1 equiv.) and K_2CO_3 (0.75 mmol, 3 equiv.) was refluxed in dry and degassed acetone (10 mL). After 16 hours, the green suspension was cooled to room temperature and filtered on a Celite pad. After removal of the solvent, the pure product was obtained as light-yellow crystals by layering of diethyl ether into a dichloromethane solution of the complex at −18 °C. Yield: 60% (light yellow crystals). ^{1}H NMR (300.1 MHz, $CDCl_3$): δ = 7.58 (d, J = 2.2 Hz, 1H, NCH), 7.39 (m, 6H, Ar), 7.20 (d, J = 2.2 Hz, 1H, NCH), 6.99–6.94 (m, 2H, Ar), 5.41 (s, 2H, CH_2), 3.74 (s, 3H, OCH_3), 1.23 (s, 9H, CH_3) ppm. Elemental analysis calcd (%) for $C_{21}H_{24}CuBrN_2O{\cdot}0.5H_2O$: C 53.34, H 5.33, N 5.92; Found: C 53.29, H 5.34, N 5.89. ESI(+)-MS (*m*/*z*): 703.19 [Cu(a^1)$_2$]$^+$. Crystals suitable for SC-XRD analysis were obtained by slow evaporation of a concentrated solution of the complex in acetone.

Synthesis of the copper(I) complex [Cu(a^1)$_2$]PF_6. A mixture of **Ha^1PF_6** (0.25 mmol, 1 equiv.), $[Cu(CH_3CN)_4]PF_6$ (0.25 mmol, 2 equiv.) and K_2CO_3 (1.50 mmol, 6 equiv.) was refluxed in dry and degassed acetonitrile (10 mL). After 16 hours, the yellow suspension was cooled to room temperature and filtered on a Celite pad. After removal of the solvent, the residue was extracted with dichloromethane, and upon filtration on Celite, the filtrate was dried under reduced pressure. The crude product was washed with water (3 × 10 mL) and dried under vacuum. Yield: 50% (light yellow crystals). ^{1}H NMR (300.1 MHz, CD_3CN): δ = 7.46–7.19 (m, 18H, Ar), 7.03 (d, J = 9.4 Hz, 2H, Ar), 5.10 (s, 4H, CH_2), 3.83 (s, 3H, OCH_3), 1.36 (s, 9H, CH_3) ppm. ^{31}P NMR (121 MHz, CD_3CN): δ = −144.63 (sept, J = 707 Hz, PF_6) ppm. Elemental analysis calcd (%) for $C_{42}H_{48}CuF_6N_4O_2P{\cdot}2H_2O$: C 56.97, H 5.92, N 6.33; Found: C 56.76, H 5.74, N 6.26. ESI(+)-MS (*m*/*z*): 703.22 [Cu(a^1)$_2$]$^+$. The low stability of the complex in solution prevented the obtainment of a good quality ^{13}C NMR spectrum; nevertheless, the carbene carbon chemical shift at δ 179.0 ppm was identified *via* a ^{13}C–^{1}H HMBC NMR spectrum.

Computational details

All calculations were performed with ORCA v5.0.3.[71,72] Molecular geometries were optimized without any symmetry constrain in the gas phase using the PBE0 functional.[73] Scalar relativistic effects were modeled using the Zeroth Order Regular Approximation (ZORA)[74] with the ZORA-Def2-SVP[75] basis set and the ZORA-Def2-TZVP[75] for copper with the RI[76] approximations with the related auxiliary basis sets (SARC/J).[77,78] The D3[79] dispersion correction with Becke-Johnson[80]

damping was used. All optimized structures were verified as true minima by the absence of negative eigenvalues in the harmonic vibrational frequency analysis.

Single point calculations were performed at the same level of theory with a ZORA-Def2-TZVPP basis set for all atoms. The absorption spectra were modeled by time-dependent DFT calculations (TD-DFT) with the ZORA-def2-TZVPP basis set and PBE0 functional. For the TD-DFT calculations 20 roots were computed and solvation effects were included with the SMD solvation model with (DCM)[81] as solvent. The Tamm-Dancoff[82] approximation was used to speed up the calculations. Intrinsic bond orbitals (IBOs)[83] were calculated, and were visualized using Chemcraft[84] and IBOview.[85]

General procedure for catalytic tests

The catalytic tests were carried out in a 10 mL Schlenk tube or, when pressure higher than 1 bar was used, in a 35 mL Fischer-Porter reactor. To the magnetic stirring bar equipped tube, after three vacuum–argon cycles, the catalyst, the solvent, the amine (substrate), and the silane were added in the order. Then, CO_2 was fluxed to saturate the environment and the reactor was closed, maintaining a CO_2 balloon connected to the reactor. For the high-pressure experiments, the reactor was simply sealed and maintained at the target pressure. Subsequently, the reactor was dipped into a thermostatic bath fixed to the target temperature. The magnetic stirring and the reactor immersion level were maintained identical in all performed tests. The starting time of the tests was set at five minutes after the reactor immersion. After the reaction time, the reactor was cooled to room temperature, depressurized, and 2,5-dimethylfuran was added with a micro syringe as internal standard (1 equiv. respect to the substrate). The reaction mixture was then thoroughly mixed and the ^{1}H NMR spectrum of a sample in $CDCl_3$ was recorded. Conversions and yields were calculated by ^{1}H NMR spectroscopy. In some cases, the addition of a small quantity of potassium carbonate to the NMR tube helped to obtain a better spectrum. Every test was performed three times and the reported conversion and yield are the resulting average value. The yield obtained in the replication of the same test varied in the range ±1%.

X-Ray crystallography

The crystallographic data for compounds **[Cu(L^1)$_2$]** and **[CuBr(a^1)]** were obtained by mounting a single crystal of each sample on a loop fiber and transferring it to a Bruker D8 Venture Photon II single crystal diffractometer equipped with an area detector, working with monochromatic MoKα radiation in the case of **[Cu(L^1)$_2$]** and CuKα radiation in the case of **[CuBr(a^1)]**. The APEX 3 program package was used to obtain the unit-cell geometrical parameters for both structures. The raw frame data were processed using SAINT and SADABS to obtain the data file of the reflections. The structures were solved using SHELXT (Intrinsic Phasing method in the APEX 3 program).[86] The refinement of the structures (based on F^2 by full-matrix least-squares techniques) was carried out using the SHELXTL-2018/3 program.[87] The hydrogen atoms were introduced in the refinement in defined geometry and refined "riding" on the corresponding carbon atoms. Deposition numbers 2371863 and 2371864 contain the supplementary crystallographic data for compound **[Cu(L^1)$_2$]** and **[CuBr(a^1)]** respectively.

Results and discussion

Synthesis and characterization

The hybrid bidentate **H$_2$L$^{1–3}$Br** and tetradentate **H$_4$L^{4}Br$_2$** ligand precursors were prepared by a two-step synthesis (Scheme 2), adaptation of a previously reported procedure,[69,88] consisting in the quaternarization of 1-(5-*tert*-butyl-2-methoxyphenyl)-imidazole with the selected alkyl halide, followed by the demethylation of the methoxy moieties using HBr. The imidazolium salts **Ha$^{1–2}$Br**, **Ha^{3}I** and **H$_2$a^{4}Br$_2$** obtained after the first reaction step, can be used as NHC precursors as well (*vide infra*). From the imidazolium salts **Ha^{1}Br** and **H$_2$L^{1}Br**, the respective hexafluorophosphate salts **Ha^{1}PF$_6$** and **H$_2$L^{1}PF$_6$** were obtained in high yield, performing the anion exchange in water using KPF_6. All the proligands were isolated with an overall yield >80%.

The ligand precursors **H$_2$L$^{1–3}$Br** and **H$_4$L^{4}Br$_2$** were reacted with $Cu(OAc)_2{\cdot}H_2O$ and K_2CO_3 in methanol to afford the

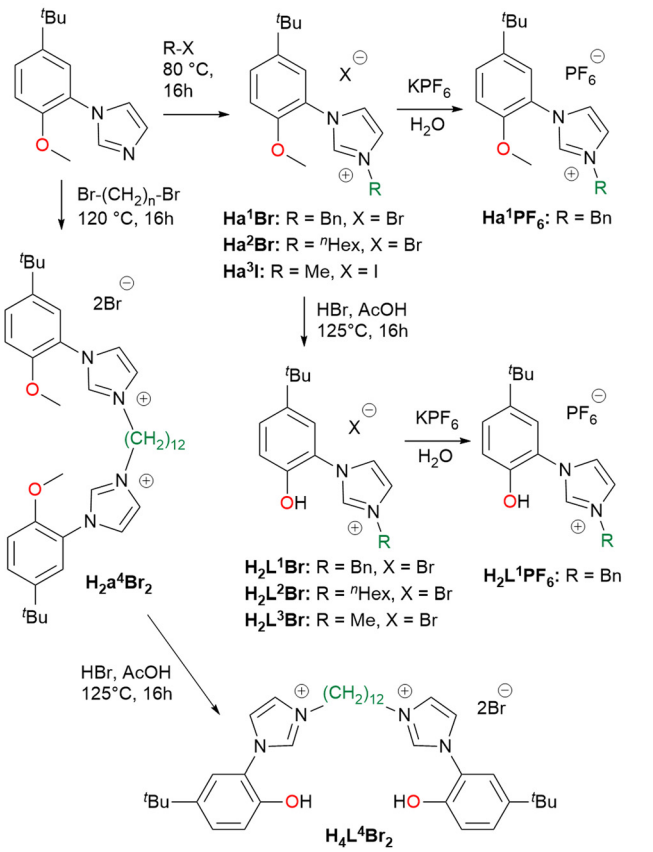

Scheme 2 Synthesis of the ligand precursors used in this study.

corresponding Cu(II) complexes of general formula $[Cu(L)_2]$ or [Cu(L)] depending on the use of bidentate ($\mathbf{L^{1-3}}$) or tetradentate ($\mathbf{L^4}$) ligands (Scheme 3). By using tetradentate ligand precursors with shorter linkers, methylene or dimethylene bridging groups,[69,70] it was not possible to isolate the corresponding Cu(II) complexes. The complexes $\mathbf{[Cu(L^{1-3})_2]}$ are soluble in common organic solvents, while $\mathbf{[Cu(L^4)]}$ is soluble only in dichloromethane, chloroform, and sparingly soluble in acetone. Complexes $\mathbf{[Cu(L^{1-3})_2]}$ and $\mathbf{[Cu(L^4)]}$ were characterized by means of ESI-MS spectrometry, FT-IR and UV-Vis spectroscopy and in the case of $\mathbf{[Cu(L^1)_2]}$ single crystal X-ray diffraction. In the ESI-MS spectra, the presence of the peaks attributed to the species $[Cu(L^{1-3})_2 + H^+]^+$ and $[Cu(L^4) + H^+]^+$ is diagnostic of the formation of the Cu(II) complexes.

In the FT-IR spectra of the complexes (Fig. S35–38†), the lack of the PhO–H stretching signal at *ca.* 3060 cm^{-1}, clearly visible for proligand $\mathbf{H_2L^1Br}$ (Fig. S34†), agrees with the deprotonation of the phenol moieties upon metal coordination. The UV-visible absorption spectra of the Cu(II) complexes were registered in dichloromethane solution, showing similar features for the four compounds with three well defined absorption maxima at *ca.* 230, 320 and 460 nm (Fig. S39–42†). Finally in the case of complex $\mathbf{[Cu(L^1)_2]}$, the molecular structure was confirmed by X-ray diffraction on a single crystal obtained by slow evaporation of an acetone solution of the complex (Fig. 1). The complex crystallizes in the monoclinic $P2_1$ space group and presents a slightly distorted square planar geometry, as indicated by the value close to 0 (0.05) of the τ_4 geometry index.[89] In the coordination sphere of the Cu(II) centre the two NHC and the two phenolate donors are mutually in *trans*.

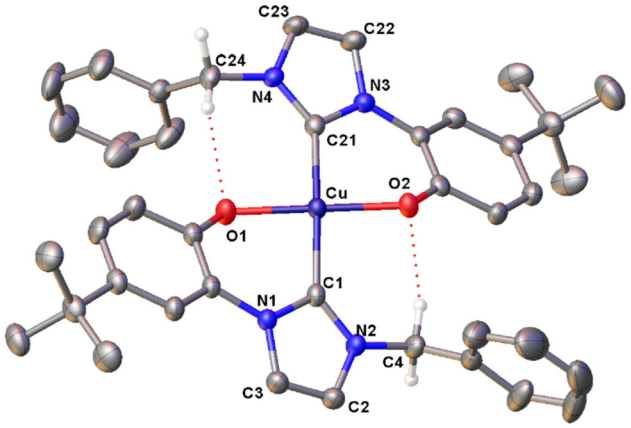

Fig. 1 ORTEP drawing of complex $\mathbf{[Cu(L^1)_2]}$. Ellipsoids are drawn at the 50% probability level. Hydrogen atoms have been omitted for clarity. Selected bond distances (Å) and angles (°): Cu–C1 2.005(3), Cu–C21 2.007(3), Cu–O1 1.946(2), Cu–O2 1.958(2), C1–Cu–C21 174.1(1), O1–Cu–O2 179.2(1), C1–Cu–O1 86.7(1), C21–Cu–O2 88.3(1), C1–Cu–O2 179.2(1), C21–Cu–O1 91.6(1).

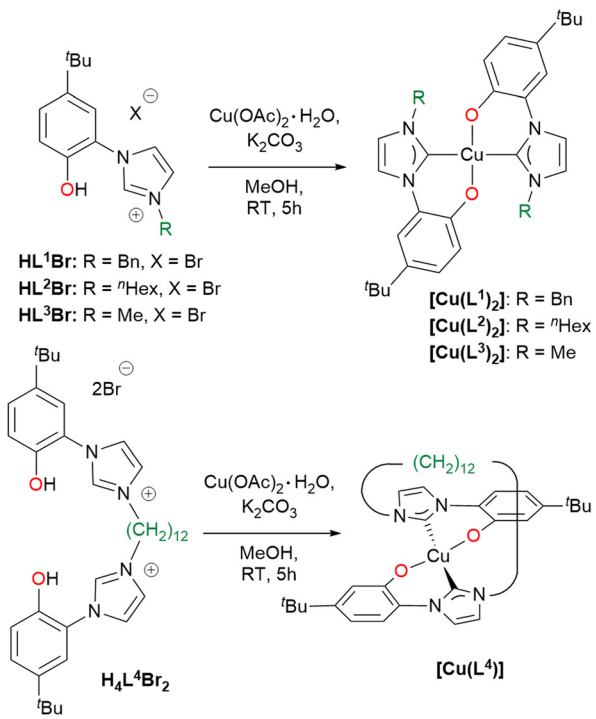

Scheme 3 Synthesis of the Cu(II) complexes prepared in this work.

The two NHC rings are almost coplanar, with a dihedral angle of 5.75(13)° between them, and are slightly tilted with respect to the mean metal coordination plane with angles of 26.82(9) and 23.03(9)° respectively. The Cu–O and Cu–C bond lengths are comparable to similar copper(II) NHC–phenolate complexes.[43] Two intramolecular C–H···O hydrogen bonds are present in the structure. The donor-H···acceptor distances (D) are 2.939(4) and 3.015 (4) for C24–H···O1 and C4–H···O2 respectively. The C–H···O angles (θ) are 124.03(17)° and 137.83(19)° for C24–H···O1 and C4–H···O2 respectively. Thus, D and θ values are within the ranges of those reported in the literature for this type of interaction.[90]

The number of homoleptic Cu(II) complexes with hybrid NHC–phenolate ligands reported in the literature up to now is very limited.[43–45] All of them exhibit a square planar coordination geometry, with different degrees of angular distortion and a *trans* arrangement. The formation of *cis* isomer has not been documented yet in these systems. Instead, with group 10 metal centres both the *cis* and *trans* isomers can be obtained selectively, mainly depending on the steric bulkiness of the NHC wingtip substituent. With methyl wingtip the *cis* isomer is obtained, whereas with bulkier Dipp (2,6-diisopropyl-phenyl) or Mes (mesityl) wingtips the *trans* isomer is isolated.[91] Our results align with the literature results for Cu(II), as indicated by the molecular structure of $\mathbf{[Cu(L^1)_2]}$ and by the fact that in the case of the tetradentate ligands, only the use of a long and flexible bridging group, allowing the formation of the *trans* isomer, brings to the isolation of a stable Cu(II) complex. Differently, in a previous work we successfully coordinated tetradentate bis(NHC)–bis(phenolate) ligands with the shorter CH_2 and CH_2CH_2 linkers to Ni(II), obtaining the complexes *cis*-[NiL].[70]

To gain more insight on the experimental selective formation of the *trans* isomer for our Cu(II) complexes, the elec-

tronic and structural properties of the complex with the benzyl substituent were investigated by means of computational methods. In order to save computational resources, the ^{t}Bu group on the phenolate ring was substituted with a methyl one, and the truncated complex is reported as $\mathbf{[Cu(L^1)_2]^{Me}}$ in the text. DFT calculations in the case of ***trans*-$\mathbf{[Cu(L^1)_2]^{Me}}$** well reproduced the structural parameters observed in the solid-state structure of $\mathbf{[Cu(L^1)_2]}$ (Fig. 2, left). The calculated τ_4 geometry index is 0.00, so perfectly square planar, close to the 0.05 value measured by XRD. Next, the geometry of the *cis* isomer was optimized at the same level of theory, obtaining for ***cis*-$\mathbf{[Cu(L^1)_2]^{Me}}$** a highly distorted structure as indicated by the τ_4 geometry index of 0.51 (Fig. 2, right). The deviation from a square planar coordination is imposed by the arrangement of the ligands forced by the steric hindrance of the benzyl wingtip substituents. A consequence of the forced *cis* geometry is the loss of the hydrogen bonding interaction evident in the X-ray structure of the *trans* isomer. In gas phase, the *trans* isomer is predicted thermodynamically more stable than the *cis* one ($\Delta G_{cis-trans}$ = +6 kJ mol^{-1}), but the energy difference is too small to justify the selective *trans* isomer formation, thus kinetic factors cannot be excluded in determining the output of the syntheses.

Next, we investigated the electronic structure of the $\mathbf{[Cu(L^1)_2]^{Me}}$ complex, and the spin-density is located mainly on the metal centre with small contribution from the ligands (see Fig. 3).

Intrinsic bonding orbital (IBO) analysis shows that in complex ***trans*-$\mathbf{[Cu(L^1)_2]^{Me}}$** the ligand forms two sigma bonds with the metal centre (see Fig. 4). In addition, TD-DFT calculations on the *cis* and *trans* isomers of $\mathbf{[Cu(L^1)_2]^{Me}}$ predict a weak absorption band for the *cis* isomer at $\lambda_{abs.}$ = 537 nm (f_{osc} = 0.016) which is not observed in the experimental UV-Vis spectrum (see Fig. S67†). Differently, the TD-DFT spectrum of the *trans* isomer well reproduces the experimental absorption spectrum with a predicted $\lambda_{abs.}$ = 405 nm (f_{osc} = 0.033) in good agreement with the experimental value of 455 nm. Therefore, we tentatively suggest that also in solution the *trans* isomer is favoured.

Successively, with the aim of comparing the catalytic activity of Cu(II) and Cu(I) complexes (*vide infra*), we tried to coordinate the hybrid ligands $\mathbf{L^{1-4}}$ to Cu(I), but none of the complexation attempts led to the desired product. Differently, by using potassium carbonate as base, [CuBr(SMe$_2$)] as metal precursor, and performing the reaction in acetone the Cu(I) complex $\mathbf{[CuBr(a^1)]}$ was obtained starting from the ligand precursor $\mathbf{Ha^1Br}$ (Scheme 4).[12] Furthermore, starting from $\mathbf{Ha^1PF_6}$ the synthesis of the bis(NHC) complex $\mathbf{[Cu(a^1)_2]PF_6}$ was achieved in acetonitrile with [Cu(CH$_3$CN)$_4$](PF$_6$) as metal source (Scheme 4). The Cu(I) complexes were isolated as crystalline light-yellow solids in moderate yields. Purity of the complexes was confirmed by elemental analysis, and from their ^{1}H NMR spectra. In the case of complex $\mathbf{[Cu(a^1)_2]PF_6}$ the carbene carbon chemical shift was identified at 179.0 ppm *via* ^{1}H–^{13}C HMBC NMR experiment, a value in agreement with other reported bis-NHC Cu(I) cationic complexes.[92]

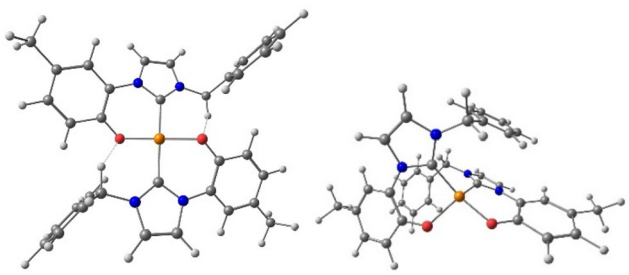

Fig. 2 Optimized structures at the ZORA PBE0 ZORA-Def2-TZVPP D3BJ level of theory level for the *trans* (left) and *cis* (right) isomers of $\mathbf{[Cu(L^1)_2]^{Me}}$. We highlight the formation of H-bonds for the *trans* isomer. Colour codes: Cu, orange; O, red; N, light blue; C, grey; H, white.

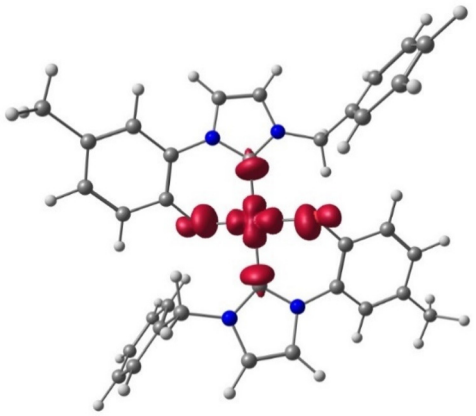

Fig. 3 Spin density plot of ***trans*-$\mathbf{[Cu(L^1)_2]^{Me}}$** ZORA PBE0 ZORA-Def2-TZVPP D3BJ level of theory (iso-surface 0.005).

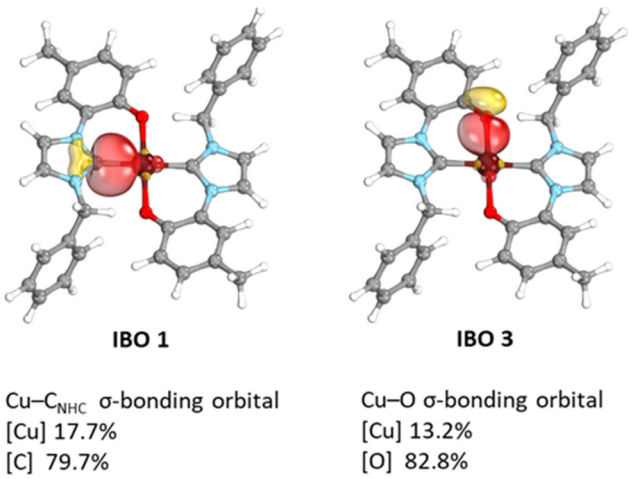

Fig. 4 IBO analysis of ***trans*-$\mathbf{[Cu(L^1)_2]^{Me}}$** complex. The metal–ligand σ-bonding orbitals are shown and the partial-charge distribution of a given IBO at ZORA PBE0 ZORA-Def2-TZVPP D3BJ level of theory is given below. Structural depictions were made using IboView. Considering the centrosymmetric structure of the complex only one Cu–C and one Cu–O σ-bonding orbitals are depicted.

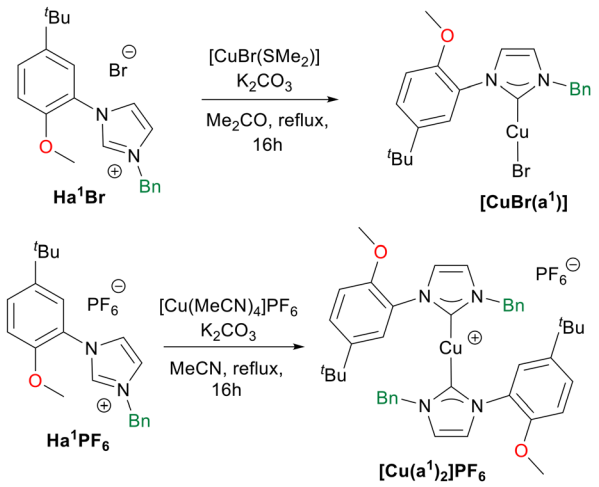

Scheme 4 Synthesis of the Cu(I) complexes prepared in this work.

The molecular structure of the complex **[CuBr(a^1)]** was confirmed by single crystal X-ray diffraction (Fig. 5), from crystals obtained from layering of diethylether on a dichloromethane solution of the complex at −18 °C. As expected, the copper(I) centre presents a slightly distorted linear geometry (C1–Cu–Br 178.3(2)°). The Cu–C and Cu–Br bond distances of 1.890(6) and 2.2273(9) Å respectively are perfectly in agreement with similar [CuBr(NHC)] complexes reported in the literature.[93] No interaction is observed between the oxygen atom of the methoxy group and the copper centre, with the substituted phenyl wingtip oriented in the way that minimizes steric repulsion around the metal centre.

Catalytic studies

The obtained Cu(II) complexes were tested as catalyst precursors in the reductive *N*-formylation and *N*-methylation of amines with CO_2, a reaction that we have recently studied with Mn(I) complexes as catalysts.[59] A preliminary screening of the reaction conditions was carried out using *N*-ethylaniline (**1a**) as substrate, **[Cu(L^1)$_2$]**, 3 equivalents of $PhSiH_3$ as reducing agent, at 40 °C and varying the reaction solvent and CO_2 pressure (Scheme 5).

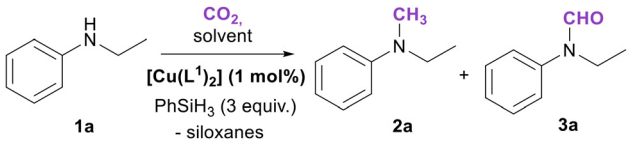

Scheme 5 Benchmark reaction for the *N*-methylation and *N*-formylation of amines with CO_2. Reaction conditions: *N*-ethylaniline 0.40 mmol, $PhSiH_3$ (3 equiv.), **[Cu(L^1)$_2$]** 1 mol%, 40 °C, 5 h, in 1 mL of solvent.

The results of the preliminary catalytic experiments are reported in Table S2.† Under the adopted reaction conditions, the proligand **H$_4$L^{1}Br$_2$** and $Cu(OAc)_2{\cdot}H_2O$ were not able to promote any product formation. Instead, using **[Cu(L^1)$_2$]** at a 1 mol% loading with respect to the aniline **1a** a complete conversion can be achieved in 5 h at 40 °C and a 3 bar CO_2 pressure, using DMF or the ionic liquid 1-butyl-2,3-dimethylimidazolium bis(trifluoromethylsulfonyl)imide ([BMMIM][NTf$_2$]) as solvent. A product mixture of **2a** and **3a** was obtained, with **3a** as the main product in all the performed tests. A blank experiment carried out using [BMMIM][NTf$_2$] showed that the ionic liquid is not able to promote the products formation in the absence of the copper complex (Table 1, entry 1). Successively, to further increase the methylated (**2a**) product yield, the temperature was increased to 60 °C, the CO_2 pressure was lowered to 1 bar, and the reaction time was extended to 16 h, performing the reaction in [BMMIM][NTf$_2$] (Table 1). Under these conditions the selectivity was reversed with **2a** being always the main product. This is not surprising since it is known that a decrease in the CO_2 pressure and an increase in the temperature shift the selectivity towards the methylated species.[59] Then the activity of the different Cu(II) complexes was evaluated (Table 1, entries 2–5).

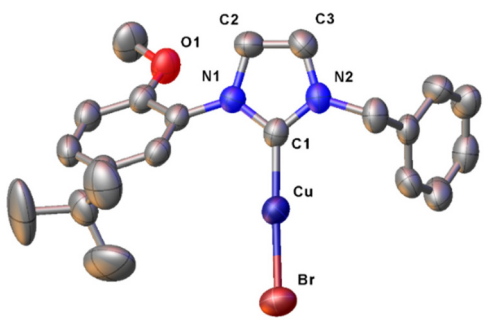

Fig. 5 ORTEP drawing of complex **[CuBr(a^1)]**. Ellipsoids are drawn at the 50% probability level. Hydrogen atoms have been omitted for clarity. Selected bond distances (Å) and angles (°): Cu–C1 1.890(6), Cu–Br 2.2273(9), C1–Cu–Br 178.3(2).

Table 1 *N*-methylation and *N*-formylation of *N*-ethylaniline with CO_2 and hydrosilanes

Entry	Catalyst	Silane (equiv.)	Conv.^{a}/%	**2a**^{a}/%	**3a**^{a}/%
1	—	$PhSiH_3$ (3)	0	0	0
2	**[Cu(L^1)$_2$]**	$PhSiH_3$ (3)	84	62	22
3	**[Cu(L^2)$_2$]**	$PhSiH_3$ (3)	100	81	19
4	**[Cu(L^3)$_2$]**	$PhSiH_3$ (3)	29	15	14
5	**[Cu(L^4)]**	$PhSiH_3$ (3)	20	15	5
6	**[CuBr(a^1)]**	$PhSiH_3$ (3)	5	2	3
7	**[Cu(a^1)$_2$]PF$_6$**	$PhSiH_3$ (3)	2	0	2
8	**[Cu(L^2)$_2$]**	Ph_2SiH_2 (3)	13	13	0
9^b	**[Cu(L^2)$_2$]**	$PhSiH_3$ (3)	68	59	9
10^b	**[Cu(L^2)$_2$]**	Ph_2SiH_2 (3)	39	39	0
11	**[Cu(L^2)$_2$]**	Ph_2SiH_2 (9)	75	75	Traces
12	**[Cu(L^2)$_2$]**	$PhSiH_3$ (6)	100	85	15
13^c	**[Cu(L^2)$_2$]**	$PhSiH_3$ (3)	100	93	7

Reaction conditions: *N*-ethylaniline 0.40 mmol, hydrosilane, catalyst loading 1 mol%, p(CO_2) = 1 bar (balloon), 60 °C, 24 h, in 1 mL of [BMMIM][NTf$_2$]. ^{a} Yield determined by ^{1}H NMR using 2,5-dimethylfuran as an internal standard. ^{b} *T* = 80 °C. ^{c} Catalyst loading 2 mol%, *t* = 16 h.

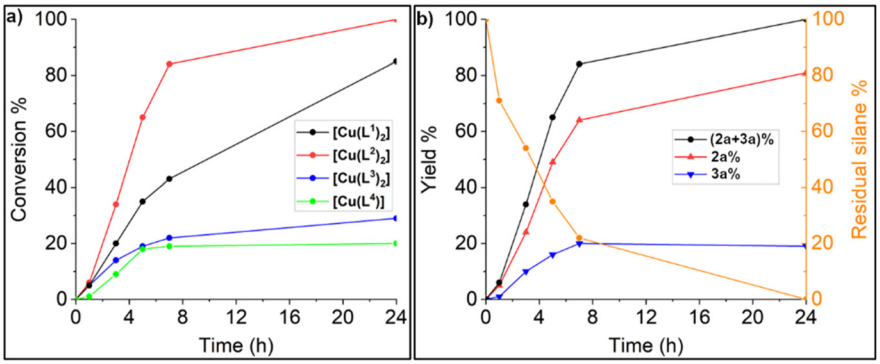

Fig. 6 (a) Total conversion of *N*-ethylaniline *versus* time using the Cu(II) complexes; (b) total conversion of *N*-ethylaniline, yield of **2a** and **3a** and residual silane *versus* time using **[Cu(L^2)$_2$]** as catalyst, complete data reported in Table S3.† Reaction conditions for all the experiments: *N*-ethylaniline 0.40 mmol, $PhSiH_3$ (3 equiv.), catalyst loading 1 mol%, p(CO_2) = 1 bar (balloon), 60 °C, in 1 mL of [BMMIM][NTf_2].

A marked difference was observed among the different complexes, with complexes bearing ligands with bulkier wingtip substituents on the NHC showing a better catalytic performance. The catalysts screening shows that **[Cu(L^2)$_2$]** is the most active and selective towards the *N*-methyl product, leading to full conversion of the aniline **1a** and an 81% yield of **2a** (Table 1, entry 3). The performance of **[Cu(L^1)$_2$]** is slightly lower compared to that of **[Cu(L^2)$_2$]**, whereas **[Cu(L^3)$_2$]** and **[Cu(L^4)]** were found to be significantly less active. The differences in activity among the Cu(II) complexes become more evident looking at Fig. 6a, in which the reagent conversion is reported against the reaction time. After 7 hours, **[Cu(L^2)$_2$]** achieved an 80% conversion, **[Cu(L^1)$_2$]** 43%, and complexes **[Cu(L^3)$_2$]** and **[Cu(L^4)]** slightly less than 20%. In Fig. 6b, the yields of **2a** and **3a** and the residual $PhSiH_3$ over time using **[Cu(L^2)$_2$]** can be observed. After 24 hours, no residual $PhSiH_3$ remains in the reaction mixture. The Cu(I) complexes **[CuBr(a^1)]** and **[Cu(a^1)$_2$]PF$_6$** were also evaluated for this reaction (Table 1, entries 6 and 7), but their performance was way lower compared to the Cu(II) complexes. The most active complex **[Cu(L^2)$_2$]** was also tested in the presence of other hydrosilanes, namely Ph_2SiH_2, Ph_3SiH, Me_2PhSiH and PMHS (polymethylhydrosiloxane). Only with Ph_2SiH_2 a poor conversion was observed (13%), interestingly with complete selectivity towards **2a** (Table 1, entry 8).

By increasing the temperature to 80 °C a different behaviour was observed with $PhSiH_3$ and Ph_2SiH_2. In the case of $PhSiH_3$ lower conversion and yields were obtained (Table 1, entry 9), probably as consequence of a faster silane consumption in side-reactions. It has been observed that at 80 °C, $PhSiH_3$ already reached 90% consumption after the first three hours (Table S3 and Fig. S46b†). Differently, in the case of Ph_2SiH_2, a higher temperature led to higher conversion and yield (39%), maintaining the full **2a** selectivity (Table 1, entry 10). Better performances can be obtained increasing the silane equivalents. With 9 Ph_2SiH_2 equivalents the **2a** yield increased to 75% (Table 1, entry 11) maintaining an almost complete selectivity. With 6 $PhSiH_3$ equivalents the **2a** yield increased to 85% (Table 1, entry 12). A better improvement was achieved maintaining 3 equivalents of silane and increasing the catalyst loading to 2 mol%, obtaining a **2a** with 93% yield (Table 1, entry 13). Under the latter conditions a preliminary substrate scope was carried out (Scheme 6).

Under the adopted conditions a full conversion of the selected secondary amines was always reached, and the respective *N*-formyl and *N*-methyl products were obtained in different ratio. The methylation of the *N*-methylaniline (**1b**) was achieved with a 92% yield. Instead, the reaction carried out using *N*-methyl-*p*-methoxyaniline (**1c**) or dibenzylamine (**1d**) led to a lower methylated product yield of 80% and 75% respectively.

Mechanistic insights

To obtain information about the mechanism of the reaction, specific reactivity tests were performed. For this reaction, the

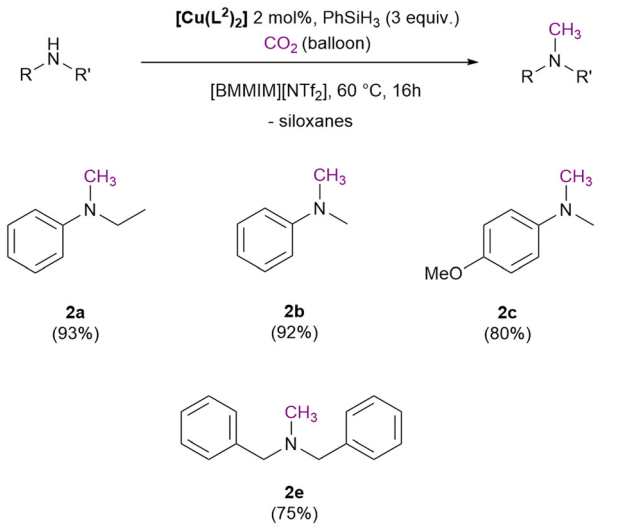

Scheme 6 *N*-Methylation of secondary amines using catalyst **[Cu(L^2)$_2$]**, yield in parenthesis. **2a**: *N*-ethyl-*N*-methylaniline, **2b**: *N*,*N*-dimethylaniline, **2c**: *N*,*N*-dimethyl-*p*-methoxyaniline, **2d**: *N*-methyl-*N*,*N*-dibenzylamine.

mechanism is still under debate and might vary for different catalysts and hydrosilanes. Both Beller and Cantat proposed that the reaction proceeds through an initial formation of silylformate from CO_2 and hydrosilane, then formation of *N*-formyl product by reaction with the amine and finally the *N*-methyl product derives from a further reduction (Scheme 7, route a).[56,57] The *N*-formyl product can be formed also *via* reduction of a carbamate salt or *via* formation of a silyl carbamate.[94,95] Alternatively, as reported by Zhang and Wang, the silylformate can react with $PhSiH_3$ to form a silyl methoxide intermediate that is attacked by the nucleophilic amine to yield the desired *N*-methylamine (Scheme 7, route b).[94,96,97] To verify if the *N*-formyl to *N*-methyl reduction mechanism (route a) is involved in our case, a test was carried out using *N*-methyl-formanilide **3a** as the substrate under catalytic conditions, showing no reaction (Scheme 8, top). Successively, two NMR scale reactions were carried out under slightly different conditions and using both $PhSiH_3$ and Ph_2SiH_2 (Scheme 8, bottom). With $PhSiH_3$ almost no reaction was observed, whereas with Ph_2SiH_2 complete conversion of **3a** into **2a** was achieved.

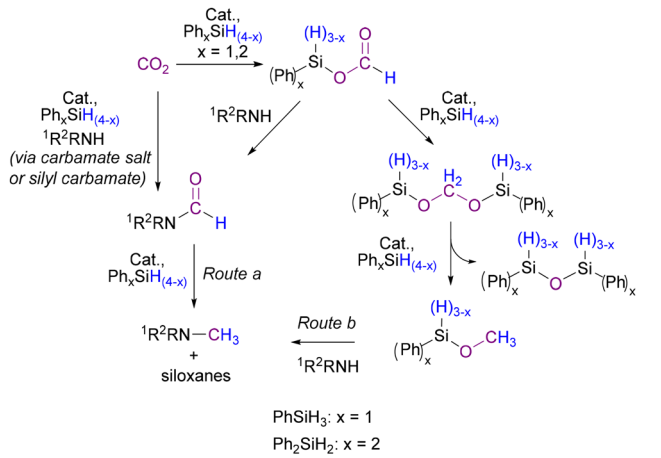

Scheme 7 Supposed reaction routes involved in the *N*-formylation and *N*-methylation of amines with CO_2 and hydrosilanes according to the literature.[56,57,94–97]

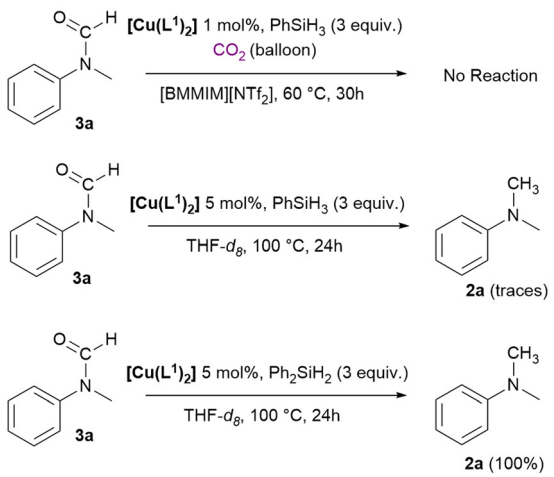

Scheme 8 Reduction attempt of *N*-methylformanilide **3a** using the catalyst $[Cu(L^1)_2]$ with hydrosilanes.

These results suggest that the reaction follows two different mechanisms with the different hydrosilanes, and this is consistent with what was observed in the catalytic study. In fact, using Ph_2SiH_2 we selectively obtained product **2a** (Table 1, entries 8, 10 and 11); if formation of **3a** is involved in the mechanism, it might be rapidly converted into **2a** when using Ph_2SiH_2, whereas its conversion does not take place with $PhSiH_3$ and for this reason a mixture of **2a** and **3a** is observed in the catalytic tests with this silane. We then tried to get information on the nature of the active catalytic species. In this frame, free NHCs are reported to be able of catalysing the *N*-methylation of amines with CO_2.[64] To assess whether the reaction mechanism involves the formation of free carbenes, experiments with the commercially available 1,3-bis(2,4,6-trimethylphenyl)-1,3-dihydro-2*H*-imidazol-2-ylidene (IMes) were performed and reported in Table 2. The use of IMes (2 mol%) led to complete conversion of **1a** with 92% yield in **2a** (Table 2, entry 2) under the used reaction conditions.

An analogous test carried out with the addition of elemental sulphur, resulted in a much lower yield (only 3% of **2a**). Sulphur, in fact, can trap the free carbenes, by forming the catalytically inactive thioureas.[98] The same tests were carried out using complex $[Cu(L^2)_2]$ (1 mol%), leading to the same conversions and product yields, with or without the addition of sulphur (Table 2, entries 4 and 5). This result suggests that free carbenes are not the active catalytic species in our system.

Successively, stoichiometric experiments were performed to test the stability of the Cu(II) complexes under reductive conditions. In fact, reductive organic transformations catalysed by Cu–NHC complexes in the presence of hydrosilanes typically involve the formation of Cu(I)–NHC hydride species [Cu(H)(NHC)] as key intermediates.[99–101] Dimeric Cu(I) NHC hydride complexes were obtained also treating Cu(II) species in the presence of free NHCs and hydrosilanes.[102] Complex $[Cu(L^2)_2]$ was treated with $PhSiH_3$ in NMR scale experiments in CD_3CN. The ^1H NMR spectrum of the complex alone did not show signals, as expected for a paramagnetic d^9 complex. After

Table 2 *N*-methylation and *N*-formylation of *N*-ethylaniline with CO_2 and phenylsilane

Entry	Catalyst (mol%)	Conv.[a]/%	**2a**[a]/%	**3a**[a]/%
1	—	0	0	0
2	IMes[b] (2)	100	92	8
3[c]	IMes[b] (2)	12	3	9
4	$[Cu(L^2)_2]$ (1)	100	81	19
5[c]	$[Cu(L^2)_2]$ (1)	100	81	19

Reaction conditions: *N*-ethylaniline 0.40 mmol, $PhSiH_3$ (3 equiv.), $p(CO_2)$ = 1 bar (balloon), 60 °C, 16 h, in 1 mL of $[BMMIM][NTf_2]$. [a] Yield determined by ^1H NMR using 2,5-dimethylfuran as an internal standard. [b] IMes = 1,3-Bis(2,4,6-trimethylphenyl)-1,3-dihydro-2*H*-imidazol-2-ylidene. [c] Addition of S_8 0.05 mol%.

the addition of $PhSiH_3$ (4 equiv.) bubbling and precipitation of a dark solid were observed, while the mixture colour shifted from brown to light yellow. Few minutes after the addition, the ^1H NMR spectrum showed a complex mixture of signals that evolved to a simpler and stable spectrum after 1 h at 60 °C (Fig. S54†). Two sets of signals were detected, that by comparison with the literature were attributed to two different **L** ligands.[70] *Via* ^1H–^{13}C HMBC experiments it was possible to detect the carbene carbon signals of these two ligands at 173.1 and 173.4 ppm (Fig. S59†). The presence of dihydrogen in solution was also observed.[103] Furthermore, a new singlet at 4.61 ppm was found, attributed to a Si–H group by ^1H–^{29}Si HMBC experiments (Fig. S54†). In the corresponding cross-peak in the ^1H–^{29}Si HMBC experiments, the ^{29}Si signal was found at −197.7 ppm. A similar ^{29}Si chemical shift was recently reported by Bellemin-Laponnaz, Mauro *et al.*, and attributed to a hexacoordinated Si(IV) NHC–O species (Fig. S60†).[104] Furthermore, in the ^1H–^1H NOESY we observed a cross-peak between the N–CH_2– protons of the NHC wingtip substituent and the new singlet at 4.61 ppm attributed to the Si–H group (Fig. S57†). All the above considerations are consistent with the formation of a species of formula $[PhSiH(L^2)_2]$. The same behaviour was also observed in the reaction between the complex $\mathbf{[Cu(L^1)_2]}$ and $PhSiH_3$, for which the formation of the analogous silicon adduct is probably involved, whereas with $\mathbf{[Cu(L^1)_2]}$ that is much less active in catalysis, the silicon adduct is not observed in the NMR experiments.

Summarizing, the performed experiments seem to indicate that the Cu(II) complexes are reduced in the presence of $PhSiH_3$. However, formation of Cu(I) hydride species typically observed in Cu(I) NHC catalysis seems not to be followed with the hybrid NHC–phenolate ligand system, whereas the formation of a silicon adduct seems to be more likely. Further studies are ongoing to clarify the details of the reaction mechanism.

Conclusions

Four new Cu(II) complexes with hybrid NHC–phenolate ligands were obtained by a convenient synthetic procedure using readily available $Cu(OAc)_2{\cdot}H_2O$ as metal precursor under mild reaction conditions. Either bidentate ($\mathbf{L^{1–3}}$) or tetradentate ($\mathbf{L^4}$) NHC–phenolate ligands can be used in the complexes preparation of general formula $\mathbf{[Cu(L^{1–3})_2]}$ and $\mathbf{[Cu(L^4)]}$ provided that the two NHC and the two phenolate donors are mutually in *trans* in the Cu(II) coordination sphere. This restricts the use of tetradentate ligands only to those presenting a long and fluxional linker between the two NHC donors, such as the dodecamethylene used in L^4.

Complexes $\mathbf{[Cu(L^{1–3})_2]}$ and $\mathbf{[CuL^4]}$ were used in the catalytic reductive *N*-formylation and *N*-methylation of amines with CO_2 and hydrosilanes, with complex $\mathbf{[Cu(L^2)_2]}$ delivering the best catalytic performance among the series of complexes synthesised in this study. An efficient reaction protocol was developed using the ionic liquid $[BMMIM][NTf_2]$ as solvent, 60 °C, 1 bar CO_2 and 3 equivalents of $PhSiH_3$. Under these conditions, it was possible to perform the *N*-methylation of secondary aromatic amines and dibenzylamine in high yield. Reactivity tests indicated that under the adopted conditions the *N*-methylation of amines follows two different reaction routes with different hydrosilanes. With $PhSiH_3$, *N*-methylation occurs probably *via* a silyl methoxide path (route b, Scheme 7), whereas with Ph_2SiH_2 the stepwise *N*-formylation to *N*-methylation is also possible (route a, Scheme 7). The study of the behaviour of the Cu(II) complexes under reductive conditions in the presence of controlled amounts of $PhSiH_3$, revealed that the starting complexes are reduced to diamagnetic species that through NMR studies were assigned to be Si(IV) adducts. Overall, the use of hybrid NHC–phenolate ligands in the reductive catalytic *N*-methylation on amines with CO_2 and hydrosilanes bring to a different reactivity compared to standard NHCs, opening new possibilities to develop innovative catalytic systems. Further studies are ongoing to fully elucidate the reaction mechanism to fully exploit the potential of these systems in catalysis.

Author contributions

Giammarco Meloni: conceptualization, investigation, data curation, writing – original draft. Luca Morgan: investigation. David Cappelletti: investigation. Matteo Bevilacqua: data curation, writing – review & editing. Claudia Graiff: investigation, writing – review & editing. Piermaria Pinter: investigation, writing – original draft. Andrea Biffis: writing – review & editing. Cristina Tubaro: conceptualization, supervision, writing – review & editing. Marco Baron: conceptualization, supervision, writing – original draft, funding acquisition.

Data availability

The data supporting this article have been included as part of the ESI.† Deposition numbers 2371863 and 2371864† contain the supplementary crystallographic data for compound $\mathbf{[Cu(L^1)_2]}$ and $\mathbf{[CuBr(a^1)]}$ respectively. These data are provided free of charge by the joint Cambridge Crystallographic Data Centre and Fachinformationszentrum Karlsruhe Access Structures service.

Conflicts of interest

There are no conflicts to declare.

Acknowledgements

We dedicate this work to our mentor prof. Marino Basato on the occasion of his 80th birthday. This work was supported by the European Union - Next Generation EU - Bando PRIN 2022 – M4. C2.1.1, project 20224PJT7C - MEGs, and by the Department of

Chemical Sciences of the University of Padova [P-DiSC#01BIRD2019-UNIPD]. Prof. Paolo Sgarbossa (University of Padova) is kindly acknowledged for the ESI-MS measurements.

References

1 A. Das, Y. Ren, C. Hessin and M. D.-E. Murr, *Beilstein J. Org. Chem.*, 2020, **16**, 858–870.
2 L.-J. Cheng and N. P. Mankad, *Chem. Soc. Rev.*, 2020, **49**, 8036–8064.
3 Y. Wang, T. Tang, Y. Yuan, N. Li, X. Wang and J. Guan, *ChemMedChem*, 2024, **19**, e202400060.
4 Y. Han, N. Xie and W. Zhou, *Adv. Ther.*, 2024, **7**, 2300305.
5 J. R. Lamichhane, E. Osdaghi, F. Behlau, J. Köhl, J. B. Jones and J.-N. Aubertot, *Agron. Sustainable Dev.*, 2018, **38**, 28.
6 A. J. I. Arduengo, H. V. R. Dias, J. C. Calabrese and F. Davidson, *Organometallics*, 1993, **12**, 3405–3409.
7 A. H. Hoveyda, Y. Zhou, Y. Shi, M. K. Brown, H. Wu and S. Torker, *Angew. Chem., Int. Ed.*, 2020, **59**, 21304–21359.
8 K. Lee, H. Wu, F. Haeffner and A. H. Hoveyda, *Organometallics*, 2012, **31**, 7823–7826.
9 J. A. Dabrowski, F. Haeffner and A. H. Hoveyda, *Angew. Chem., Int. Ed.*, 2013, **52**, 7694–7699.
10 F. Gao, J. L. Carr and A. H. Hoveyda, *J. Am. Chem. Soc.*, 2014, **136**, 2149–2161.
11 N. W. Mszar, F. Haeffner and A. H. Hoveyda, *J. Am. Chem. Soc.*, 2014, **136**, 3362–3365.
12 O. Santoro, A. Collado, A. M. Z. Slawin, S. P. Nolan and C. S. J. Cazin, *Chem. Commun.*, 2013, **49**, 10483–10485.
13 S. Díez-González, E. D. Stevens and S. P. Nolan, *Chem. Commun.*, 2008, 4747–4749.
14 S. Díez-González, A. Correa, L. Cavallo and S. P. Nolan, *Chem. – Eur. J.*, 2006, **12**, 7558–7564.
15 H. Kaur, F. K. Zinn, E. D. Stevens and S. P. Nolan, *Organometallics*, 2004, **23**, 1157–1160.
16 M. R. L. Furst and C. S. J. Cazin, *Chem. Commun.*, 2010, **46**, 6924–6925.
17 F. Lazreg, A. M. Z. Slawin and C. S. J. Cazin, *Organometallics*, 2012, **31**, 7969–7975.
18 F. Lazreg, F. Nahra and C. S. J. Cazin, *Coord. Chem. Rev.*, 2015, **293–294**, 48–79.
19 J. D. Egbert, C. S. J. Cazin and S. P. Nolan, *Catal. Sci. Technol.*, 2013, **3**, 912–926.
20 O. Santoro, F. Lazreg, D. B. Cordes, A. M. Z. Slawin and C. S. J. Cazin, *Dalton Trans.*, 2016, **45**, 4970–4973.
21 H. D. Velázquez, Y. R. García, M. Vandichel, A. Madder and F. Verpoort, *Org. Biomol. Chem.*, 2014, **12**, 9350–9356.
22 K. S. Egorova and V. P. Ananikov, *Organometallics*, 2017, **36**, 4071–4090.
23 K. M. P. Wheelhouse, R. L. Webster and G. L. Beutner, *Organometallics*, 2023, **42**, 1677–1679.
24 M. Albrecht, R. Bedford and B. Plietker, *Organometallics*, 2014, **33**, 5619–5621.
25 J. Beaudelot, S. Oger, S. Peruško, T.-A. Phan, T. Teunens, C. Moucheron and G. Evano, *Chem. Rev.*, 2022, **122**, 16365–16609.
26 M. J. Leitl, V. A. Krylova, P. I. Djurovich, M. E. Thompson and H. Yersin, *J. Am. Chem. Soc.*, 2014, **136**, 16032–16038.
27 J. Nitsch, F. Lacemon, A. Lorbach, A. Eichhorn, F. Cisnetti and A. Steffen, *Chem. Commun.*, 2016, **52**, 2932–2935.
28 M. Elie, F. Sguerra, F. Di Meo, M. D. Weber, R. Marion, A. Grimault, J.-F. Lohier, A. Stallivieri, A. Brosseau, R. B. Pansu, J.-L. Renaud, M. Linares, M. Hamel, R. D. Costa and S. Gaillard, *ACS Appl. Mater. Interfaces*, 2016, **8**, 14678–14691.
29 M. Gernert, U. Müller, M. Haehnel, J. Pflaum and A. Steffen, *Chem. – Eur. J.*, 2017, **23**, 2206–2216.
30 J. Föller, C. Ganter, A. Steffen and C. M. Marian, *Inorg. Chem.*, 2019, **58**, 5446–5456.
31 C. E. Housecroft and E. C. Constable, *J. Mater. Chem. C*, 2022, **10**, 4456–4482.
32 X. Hu, I. Castro-Rodriguez and K. Meyer, *J. Am. Chem. Soc.*, 2003, **125**, 12237–12245.
33 D. I. Bezuidenhout, G. Kleinhans, G. Guisado-Barrios, D. C. Liles, G. Ung and G. Bertrand, *Chem. Commun.*, 2014, **50**, 2431–2433.
34 Y. Liu, S. G. Resch, I. Klawitter, G. E. Cutsail III, S. Demeshko, S. Dechert, F. E. Kühn, S. DeBeer and F. Meyer, *Angew. Chem., Int. Ed.*, 2020, **59**, 5696–5705.
35 N. Ségaud, J. McMaster, G. van Koten and M. Albrecht, *Inorg. Chem.*, 2019, **58**, 16047–16058.
36 B. Liu, B. Liu, Y. Zhou and W. Chen, *Organometallics*, 2010, **29**, 1457–1464.
37 B. R. M. Lake and C. E. Willans, *Organometallics*, 2014, **33**, 2027–2038.
38 M. Sharma, B. Adhikari, R. F. Awoyemi, A. M. Perkins, A. K. Duckworth, B. Donnadieu, D. O. Wipf, S. L. Stokes and J. P. Emerson, *Chemistry*, 2022, **4**, 560–575.
39 J. Cheng, L. Wang, P. Wang and L. Deng, *Chem. Rev.*, 2018, **118**, 9930–9987.
40 E. Jürgens, O. Back, J. J. Mayer, K. Heinze and D. Kunz, *Z. Naturforsch., B: J. Chem. Sci.*, 2016, **71**, 1011–1018.
41 D. J. O'Hearn and R. D. Singer, *Organometallics*, 2017, **36**, 3175–3177.
42 M. Sharma, A. M. Perkins, R. F. Awoyemi, A. N. Schmittou, S. Raju, B. S. Pierce, B. Donnadieu, D. O. Wipf, S. L. Stokes and J. P. Emerson, *Dalton Trans.*, 2024, **53**, 3180–3190.
43 I. Ahmad Bhat, I. Avinash, S. Kumar Sachan, S. Singh and G. Anantharaman, *Eur. J. Inorg. Chem.*, 2021, **2021**, 4560–4565.
44 A. O. Larsen, W. Leu, C. N. Oberhuber, J. E. Campbell and A. H. Hoveyda, *J. Am. Chem. Soc.*, 2004, **126**, 11130–11131.
45 A. J. Boydston and C. W. Bielawski, *Polym. Prepr. (Am. Chem. Soc., Div. Polym. Chem.)*, 2006, **47**, 177–178.
46 W. Eschweiler, *Ber. Dtsch. Chem. Ges.*, 1905, **38**, 880–882.
47 H. T. Clarke, H. B. Gillespie and S. Z. Weisshaus, *J. Am. Chem. Soc.*, 1933, **55**, 4571–4587.
48 E. Farkas and C. J. Sunman, *J. Org. Chem.*, 1985, **50**, 1110–1112.

49 J. R. Harding, J. R. Jones, S.-Y. Lu and R. Wood, *Tetrahedron Lett.*, 2002, **43**, 9487–9488.
50 V. Goyal, G. Naik, A. Narani, K. Natte and R. V. Jagadeesh, *Tetrahedron*, 2021, **98**, 132414.
51 Z. Guo, T. Pang, L. Yan, X. Wei, J. Chao and C. Xi, *Green Chem.*, 2021, **23**, 7534–7538.
52 T. Irrgang and R. Kempe, *Chem. Rev.*, 2020, **120**, 9583–9674.
53 D. Wang, W. Lang, W. Wang, Q. Zou, C. Yang, F. Liu and T. Zhao, *ACS Omega*, 2023, **8**, 30640–30645.
54 W. Tarpey, H. Hauptmann, B. M. Tolbert and H. Rapoport, *J. Am. Chem. Soc.*, 1950, **72**, 5126–5127.
55 W. Eschweiler, *Ber. Dtsch. Chem. Ges.*, 1905, **38**, 880–882.
56 O. Jacquet, X. Frogneux, C. D. N. Gomes and T. Cantat, *Chem. Sci.*, 2013, **4**, 2127–2131.
57 Y. Li, X. Fang, K. Junge and M. Beller, *Angew. Chem., Int. Ed.*, 2013, **52**, 9568–9571.
58 K. Beydoun, T. vom Stein, J. Klankermayer and W. Leitner, *Angew. Chem., Int. Ed.*, 2013, **52**, 9554–9557.
59 C. Masaro, G. Meloni, M. Baron, C. Graiff, C. Tubaro and B. Royo, *Chem. – Eur. J.*, 2023, **29**, e202302273.
60 T. Oku, Y. Arita, H. Tsuneki and T. Ikariya, *J. Am. Chem. Soc.*, 2004, **126**, 7368–7377.
61 I. Sorribes, K. Junge and M. Beller, *Chem. – Eur. J.*, 2014, **20**, 7878–7883.
62 S. Savourey, G. Lefèvre, J.-C. Berthet and T. Cantat, *Chem. Commun.*, 2014, **50**, 14033–14036.
63 Y. Li, I. Sorribes, C. Vicent, K. Junge and M. Beller, *Chem. – Eur. J.*, 2015, **21**, 16759–16763.
64 S. Das, F. D. Bobbink, G. Laurenczy and P. J. Dyson, *Angew. Chem., Int. Ed.*, 2014, **53**, 12876–12879.
65 K. Motokura, N. Takahashi, A. Miyaji, Y. Sakamoto, S. Yamaguchi and T. Baba, *Tetrahedron*, 2014, **70**, 6951–6956.
66 Z. Song, J. Liu, S. Xing, X. Shao, J. Li, J. Peng and Y. Bai, *Org. Biomol. Chem.*, 2023, **21**, 832–837.
67 S. Zhang, Q. Mei, H. Liu, H. Liu, Z. Zhang and B. Han, *RSC Adv.*, 2016, **6**, 32370–32373.
68 C. Qiao, X.-F. Liu, X. Liu and L.-N. He, *Org. Lett.*, 2017, **19**, 1490–1493.
69 G. Meloni, L. Beghetto, M. Baron, A. Biffis, P. Sgarbossa, M. Mba, P. Centomo, L. Orian, C. Graiff and C. Tubaro, *Mol. Catal.*, 2023, **538**, 113006.
70 G. Meloni, M. Bevilacqua, C. Graiff, A. Biffis, M. Baron and C. Tubaro, *Inorg. Chim. Acta*, 2024, **569**, 122096.
71 F. Neese, *Wiley Interdiscip. Rev.: Comput. Mol. Sci.*, 2012, **2**, 73–78.
72 F. Neese, *Wiley Interdiscip. Rev.: Comput. Mol. Sci.*, 2022, **12**, e1606.
73 C. Adamo and V. Barone, *J. Chem. Phys.*, 1999, **110**, 6158–6170.
74 C. van Wüllen, *J. Chem. Phys.*, 1998, **109**, 392–399.
75 F. Weigend and R. Ahlrichs, *Phys. Chem. Chem. Phys.*, 2005, **7**, 3297–3305.
76 F. Neese, *J. Comput. Chem.*, 2003, **24**, 1740–1747.
77 J. D. Rolfes, F. Neese and D. A. Pantazis, *J. Comput. Chem.*, 2020, **41**, 1842–1849.
78 F. Weigend, *Phys. Chem. Chem. Phys.*, 2006, **8**, 1057–1065.
79 S. Grimme, J. Antony, S. Ehrlich and H. Krieg, *J. Chem. Phys.*, 2010, **132**, 154104.
80 S. Grimme, S. Ehrlich and L. Goerigk, *J. Comput. Chem.*, 2011, **32**, 1456–1465.
81 C. J. Cramer and D. G. Truhlar, *Acc. Chem. Res.*, 2008, **41**, 760–768.
82 S. Hirata and M. Head-Gordon, *Chem. Phys. Lett.*, 1999, **314**, 291–299.
83 G. Knizia, *J. Chem. Theory Comput.*, 2013, **9**, 4834–4843.
84 Chemcraft – graphical software for visualization of quantum chemistry computations. Version 1.8, build 682. **https://www.chemcraftprog.com**.
85 G. Knizia and J. E. M. N. Klein, *Angew. Chem., Int. Ed.*, 2015, **54**, 5518–5522.
86 G. M. Sheldrick, *Acta Crystallogr., Sect. A: Found. Adv.*, 2015, **71**, 3–8.
87 G. M. Sheldrick, *Acta Crystallogr., Sect. C: Struct. Chem.*, 2015, **71**, 3–8.
88 N. Komiya, A. Yoshida and T. Naota, *Inorg. Chem. Commun.*, 2013, **27**, 122–126.
89 L. Yang, D. R. Powell and R. P. Houser, *Dalton Trans.*, 2007, 955–964.
90 G. R. Desiraju, *Acc. Chem. Res.*, 1996, **29**, 441–449.
91 I. A. Bhat, I. Avinash and G. Anantharaman, *Organometallics*, 2019, **38**, 1699–1708.
92 A. Banerjee, S. Sarkar, J. A. Shah, N. C. Frederiks, E. A. Bazan-Bergamino, C. J. Johnson and M.-Y. Ngai, *Angew. Chem., Int. Ed.*, 2022, **61**, e202113841.
93 M. Delgado-Rebollo, C. García-Morales, C. Maya, A. Prieto, A. M. Echavarren and P. J. Pérez, *J. Organomet. Chem.*, 2019, **898**, 120856.
94 H. Lv, Q. Xing, C. Yue, Z. Lei and F. Li, *Chem. Commun.*, 2016, **52**, 6545–6548.
95 Z.-Z. Yang, B. Yu, H. Zhang, Y. Zhao, G. Ji and Z. Liu, *RSC Adv.*, 2015, **5**, 19613–19619.
96 S. N. Riduan, J. Y. Ying and Y. Zhang, *ChemCatChem*, 2013, **5**, 1490–1496.
97 F. Huang, G. Lu, L. Zhao, H. Li and Z.-X. Wang, *J. Am. Chem. Soc.*, 2010, **132**, 12388–12396.
98 H. Rodríguez, G. Gurau, J. D. Holbrey and R. D. Rogers, *Chem. Commun.*, 2011, **47**, 3222–3224.
99 O. Santoro, F. Lazreg, Y. Minenkov, L. Cavallo and C. S. J. Cazin, *Dalton Trans.*, 2015, **44**, 18138–18144.
100 S. Díez-González, E. D. Stevens, N. M. Scott, J. L. Petersen and S. P. Nolan, *Chem. – Eur. J.*, 2008, **14**, 158–168.
101 M. Trose, F. Lazreg, T. Chang, F. Nahra, D. B. Cordes, A. M. Z. Slawin and C. S. J. Cazin, *ACS Catal.*, 2017, **7**, 238–242.
102 N. P. Mankad, D. S. Laitar and J. P. Sadighi, *Organometallics*, 2004, **23**, 3369–3371.
103 S. Semwal, A. Kumar and J. Choudhury, *Catal. Sci. Technol.*, 2018, **8**, 6137–6142.
104 T. Thierry, V. Giuso, F. Polo, P. Mercandelli, Y.-T. Chen, C.-H. Chang, M. Mauro and S. Bellemin-Laponnaz, *Dalton Trans.*, 2024, **53**, 6445–6450.